Design, simulation and experimental validation of a novel flexible neural probe for deep brain stimulation and multichannel recording

2012 J. Neural Eng. 9 036001

(http://iopscience.iop.org/1741-2552/9/3/036001)

J. Neural Eng. **9** (2012) 036001 (15pp) doi:10.1088/1741-2560/9/3/036001

Design, simulation and experimental validation of a novel flexible neural probe for deep brain stimulation and multichannel recording

Hsin-Yi Lai[1], Lun-De Liao[1,2], Chin-Teng Lin[1,2,3,4], Jui-Hsiang Hsu[3], Xin He[1,5], You-Yin Chen[1,6,11], Jyh-Yeong Chang[1], Hui-Fen Chen[7], Siny Tsang[8] and Yen-Yu I Shih[9,10]

[1] Department of Electrical Engineering, National Chiao Tung University, No 1001, Ta-Hsueh Rd, Hsinchu 300, Taiwan, Republic of China
[2] Brain Research Center, National Chiao Tung University, No 1001, Ta-Hsueh Rd, Hsinchu 300, Taiwan, Republic of China
[3] Department of Computer Science, National Chiao Tung University, No 1001, Ta-Hsueh Rd, Hsinchu 300, Taiwan, Republic of China
[4] Institute of Imaging and Biomedical Photonics, National Chiao Tung University Tainan Campus, No 301, Gaofa 3rd Rd, Guiren Township, Tainan 711, Taiwan, Republic of China
[5] School of Electronics Engineering and Computer Science, Peking University, No 5 Yiheyuan Rd, Haidian Dt, Beijing 100871, People's Republic of China
[6] Department of Biomedical Engineering, National Yang Ming University, No 155, Sec 2, Linong St, Taipei 112, Taiwan, Republic of China
[7] Department of Electrical Engineering, National Taiwan University, No 1, Sec 4, Roosevelt Rd, Taipei 106, Taiwan, Republic of China
[8] Department of Psychology, University of Virginia, No 102 Gilmer Hall, PO Box 400400, Charlottesville, VA 22904-4400, USA
[9] Department of Neurology, University of North Carolina, Chapel Hill, NC 27599, USA
[10] Biomedical Research Imaging Center, University of North Carolina, Chapel Hill, NC 27599, USA

E-mail: irradiance@so-net.net.tw

Received 7 October 2011
Accepted for publication 27 February 2012
Published 10 April 2012
Online at stacks.iop.org/JNE/9/036001

Abstract
An implantable micromachined neural probe with multichannel electrode arrays for both neural signal recording and electrical stimulation was designed, simulated and experimentally validated for deep brain stimulation (DBS) applications. The developed probe has a rough three-dimensional microstructure on the electrode surface to maximize the electrode–tissue contact area. The flexible, polyimide-based microelectrode arrays were each composed of a long shaft (14.9 mm in length) and 16 electrodes (5 μm thick and with a diameter of 16 μm). The ability of these arrays to record and stimulate specific areas in a rat brain was evaluated. Moreover, we have developed a finite element model (FEM) applied to an electric field to evaluate the volume of tissue activated (VTA) by DBS as a function of the stimulation parameters. The signal-to-noise ratio ranged from 4.4 to 5 over a 50 day recording period, indicating that the laboratory-designed neural probe is reliable and may be used successfully for long-term recordings. The somatosensory evoked potential (SSEP) obtained by thalamic stimulations and *in vivo* electrode–electrolyte interface impedance measurements was stable

[11] Author to whom any correspondence should be addressed.

for 50 days and demonstrated that the neural probe is feasible for long-term stimulation. A strongly linear (positive correlation) relationship was observed among the simulated VTA, the absolute value of the SSEP during the 200 ms post-stimulus period (ΣSSEP) and c-*Fos* expression, indicating that the simulated VTA has perfect sensitivity to predict the evoked responses (c-*Fos* expression). This laboratory-designed neural probe and its FEM simulation represent a simple, functionally effective technique for studying DBS and neural recordings in animal models.

(Some figures may appear in colour only in the online journal)

1. Introduction

Electrical stimulation of the nervous system has been used to treat a variety of neurological disorders (Montgomery and Gale 2008) and to facilitate lesion markings of tissues or cells of interest (Brozoski *et al* 2006, Townsend *et al* 2002). More than 60 000 patients with movement disorders worldwide have been treated by deep brain stimulation (DBS) (Hamani *et al* 2010). To understand the mechanism of DBS and to investigate possible hypotheses, comprehensive long-term recording and stimulation studies in rodent models must be developed.

Micromachining techniques have been widely applied to fabricate various new microelectrode array designs with higher accuracy rates and smaller electrode sizes (Chen *et al* 2009, Motta and Judy 2005). The most common silicon-based microelectrode arrays have been fabricated with silicon as the structural support layer, silicon nitride and silicon dioxide as the insulator and iridium or gold as the electrode material (Anderson *et al* 1989, Ensell *et al* 1996, Tanghe and Wise 1992). In addition, long-term biocompatibility and component durability are issues of concern for microelectrode arrays (Joseph and Fins 2009, Maged *et al* 2006, Stamatios and Peter 2007). An inflammation response at the implant site caused by micromotion at the tissue–electrode interface has been a major issue in the application of stiff (silicon or glass substrate) microelectrode arrays for long-term recording (Cheung 2007, Polikov *et al* 2005). The probes in previous studies that were manufactured with micromachining techniques were composed of hard substrates; thus, they easily damaged the tissue during implantation into the deep brain (Snow *et al* 2006). A probe based on flexible polyimide substrates can reduce micromotion and alleviate tissue encapsulation, thereby benefiting long-term applications (Cheung *et al* 2007).

However, most polyimide-based microelectrode arrays are prone to bending and moving from the desired implant site during implantation (Cheung *et al* 2007, Rousche *et al* 2001). Although the microelectrode arrays may be strengthened by adopting a thicker polyimide, a thicker device may cause greater harm to the tissue. Hence, the probe must be strong enough to withstand insertion forces for targeting accuracy. Furthermore, the signal-to-noise ratio (SNR) is proportional to both thermal noise and signal loss through shunt pathways (Cheung 2007, Ludwig *et al* 2006); the SNR would be improved by reducing the electrode impedance. However, a trade-off relationship between electrode impedance and an electrode's effective surface area has been identified (Paik *et al* 2003). Although the electrode impedance could be reduced by directly increasing the geometric area of the electrode, electrodes with large geometric areas would increase the overall probe size. Hence, increasing the roughness of the electrode surface has become the most intuitive approach to increase its effective surface area without increasing the geometric area of the electrode (De Haro *et al* 2002, Lee *et al* 2002, Paik *et al* 2003).

Several microfabricated microelectrode arrays have been created with high accuracy, and they can be produced with multiple channels without a significant increase to the overall probe size; however, those were generally weak in long-term stimulation (Branner *et al* 2004, Chen *et al* 2009, Motta and Judy 2005). An electric current passing through an electrode causes an irreversible electrochemical reaction that removes metallic ions from the electrode surface (Branner *et al* 2004, Lee *et al* 2002). This electromigration may reduce the quality of recorded neural signals, which may even lead to recording and stimulation failure (Branner and Normann 2000, Chen *et al* 2009). Accordingly, an increase in the thickness of the electrode is required to increase the resistance to electromigration (Motta and Judy 2005).

Moreover, the use of microfabrication techniques for DBS implants is not trivial, considering the long shanks needed to reach the subthalamic nucleus (depth: >10 mm) and other deep brain areas. The microelectrode array must be composed of probes with small cross-sectional areas to minimize brain damage (Wei and Grill 2005). To overcome the shortcomings of existing devices (Motta and Judy 2005, Maged *et al* 2006, Branner *et al* 2004, Branner and Normann 2000), a novel neural probe suitable for application in the DBS domain is needed.

Although DBS has succeeded in research and clinical applications, the effects of DBS at the neuronal level are still difficult to measure and predict (Butson and McIntyre 2005, Butson *et al* 2006, McIntyre *et al* 2004b). After surgical implantation of an electrode into the brain, electrode impedance typically increases due to the foreign-body reaction in which proteins and cells attach directly to the electrode, developing an encapsulation layer around the implanted device (Szarowski *et al* 2003, Biran *et al* 2005, Johnson *et al* 2005, Grill and Thomas Mortimer 1994, Williams *et al* 2007, Moss *et al* 2004, Haberler *et al* 2000, Xu *et al* 1997). The foreign-body reaction and electrode–tissue impedance generally stabilize several weeks post-surgery (Lempka *et al* 2009, Grill and Thomas Mortimer 1994); this stability can be perturbed with electrical stimulation (Johnson *et al* 2005, Lempka *et al* 2009, Otto *et al* 2006). Clinical measurements have also shown

reversible decreases in DBS electrode impedance following electrical stimulation (Hemm *et al* 2004).

A topic of fundamental importance to understanding the neural response to DBS is the characterization of the electric field generated by DBS and the simulation of the interactions at the electrode–tissue interface (Butson and McIntyre 2005, 2006). However, this type of analysis would be difficult, if not impossible, to perform experimentally. As previously described, finite element modeling (FEM), such as electric field models and the multi-compartment cable model for neurons, has provided the ability to quantitatively evaluate the neural response to DBS in a simulated environment (Butson and McIntyre 2006, 2008, Butson *et al* 2006, Maks *et al* 2009, McIntyre *et al* 2004a). The activating function (AF) of the extracellular potentials has been used to estimate the volume of tissue activated (VTA) (McIntyre and Grill 2000, McIntyre *et al* 2004a, Wei and Grill 2005). However, several studies have remarked that VTA estimations using the excitation threshold (ET) are more accurate than those applying AFs (Butson and McIntyre 2006, Moffitt *et al* 2004, Stamatios and Peter 2007). The ET is defined as the minimum voltage that generates action potentials in the neuronal elements and is obtained by simulating the cable model for specialized types of neurons.

The long-term functionality of electrodes used for recording and stimulation in the brain is commonly assumed to be highly dependent on the composition of the complex environment surrounding an implanted electrode. However, a shortage of quantitative information and experimentally validated methods describing the electrode–tissue interface limits the ability to design successful chronic recording and stimulation devices. In this study, a novel implantable and flexible polyimide-based neural probe is proposed and tested for reliability for usage in DBS applications on animals. Specifically, this study utilized computational models and experimental techniques to investigate how the sensitivity of VTA values affects electrode performance during chronic recording and stimulation applications. FEM was used to characterize the laboratory-designed neural probe; brain tissue properties were used to predict how the probe would be affected by the electric field generated for DBS. Furthermore, the laboratory-designed neural probes were successfully implanted into the rat brain to measure neural signals and stimulate the thalamus *in vivo*.

2. Materials and methods

2.1. Fabrication of a neural probe

Figure 1 shows the flow diagram for the fabrication process of a probe with four electrodes. Three masks were used to fabricate this probe. The first mask (M-1) was used to construct the site bases of the electrode/connector pads and the interconnecting traces of the neural probe. The second mask (M-2) formed the three-dimensional (3D) recording electrodes and connector pads. The third mask (M-3) was used to shape the neural probe, including the shaft and the angle of its tip. First, a 200 nm thick chrome layer and then a 700 nm thick copper layer were sputtered (Vvs-70L, VICTOR Taichung Machinery Works Corp., Ltd, Taiwan) as the sacrificial layer onto a glass wafer. Next, a 30 μm thick polyimide (PI-2611, HD Microsystems, USA) layer was coated onto the sacrificial layer with a spin coater (Model KW-4A, CHEMAT Technology, Inc., Taiwan) (Madou 2002, Pratap and Arunkumar 2007).

The impact resistance layer of the neural probe was subsequently created by depositing a 200 nm thick chrome layer onto the cured polyimide. The photoresist (EPG512, Everlight Chemical Industrial Corp., Taiwan) was then spun onto the impact resistance layer. Afterwards, M-3 was aligned and exposed. A chrome etchant (eSolv EG-201, Demand International Corp., Taiwan) was used to pattern the outline of the neural probe, as shown in figure 1(A). The trace layer is shown in figure 1(B). A second 30 μm thick polyimide layer was coated onto this layer and cured as described previously. Next, a 100 nm thick chrome layer and a 700 nm thick copper layer were sputtered onto the second polyimide layer with a reactor. M-1 was used to lithographically pattern the metal circuits, the 16 pairs of electrode/connector pads and the interconnecting traces. The chrome and copper were then etched, forming the structures of the metal circuits (Madou 2012).

Next, the insulation procedure was performed. A thin, third layer of polyimide (3.2 μm thick) was spun onto the trace layer for the protection of the metal circuits. Windows (3.2 μm thick) lithographically patterned with M-2 were created using O_2 plasma etching on the third layer of the polyimide, forming the 16 electrode/connector pad pair sites, as shown in figure 1(C). The electrodes and connector pads were created using electroplating. A 5 μm thick gold layer was subsequently deposited onto the electrode sites and connector pads, as shown in figure 1(D). The outline of the neural probe was lithographically patterned with M-3, which was etched with O_2 plasma (Madou 1997). The sacrificial layer was selectively etched with a copper etchant (RTE-Cu29 WBL-B, Resound Tech. Inc., Taiwan) in the final stage of fabrication. Finally, the neural probe was removed from the glass wafer, as shown in figure 1(E).

A schematic view of the neural probe is presented in figure 1(F). The tip of the probe was designed with a 50° tapered angle. In addition, the flexible, polyimide-based microelectrode array consisted of a long shaft (14.9 mm in length) and 16 electrodes (5 μm in thickness and with a diameter of 16 μm). The space between each electrode was 74 μm and the total recording length was 1.1 mm.

2.2. Measurements of in vitro impedance

The impedance of each electrode on the neural probe was assessed using impedance spectroscopy (LCR4235, Wayne Kerr Electronics Ltd, UK). After immersion in a phosphate-buffered saline (PBS) solution, the *in vitro* impedance of the neural probe was measured by applying a 20 mV sinusoidal voltage with frequencies varying from 10 Hz to 10 kHz. A large Ag/AgCl electrode was used as the reference electrode.

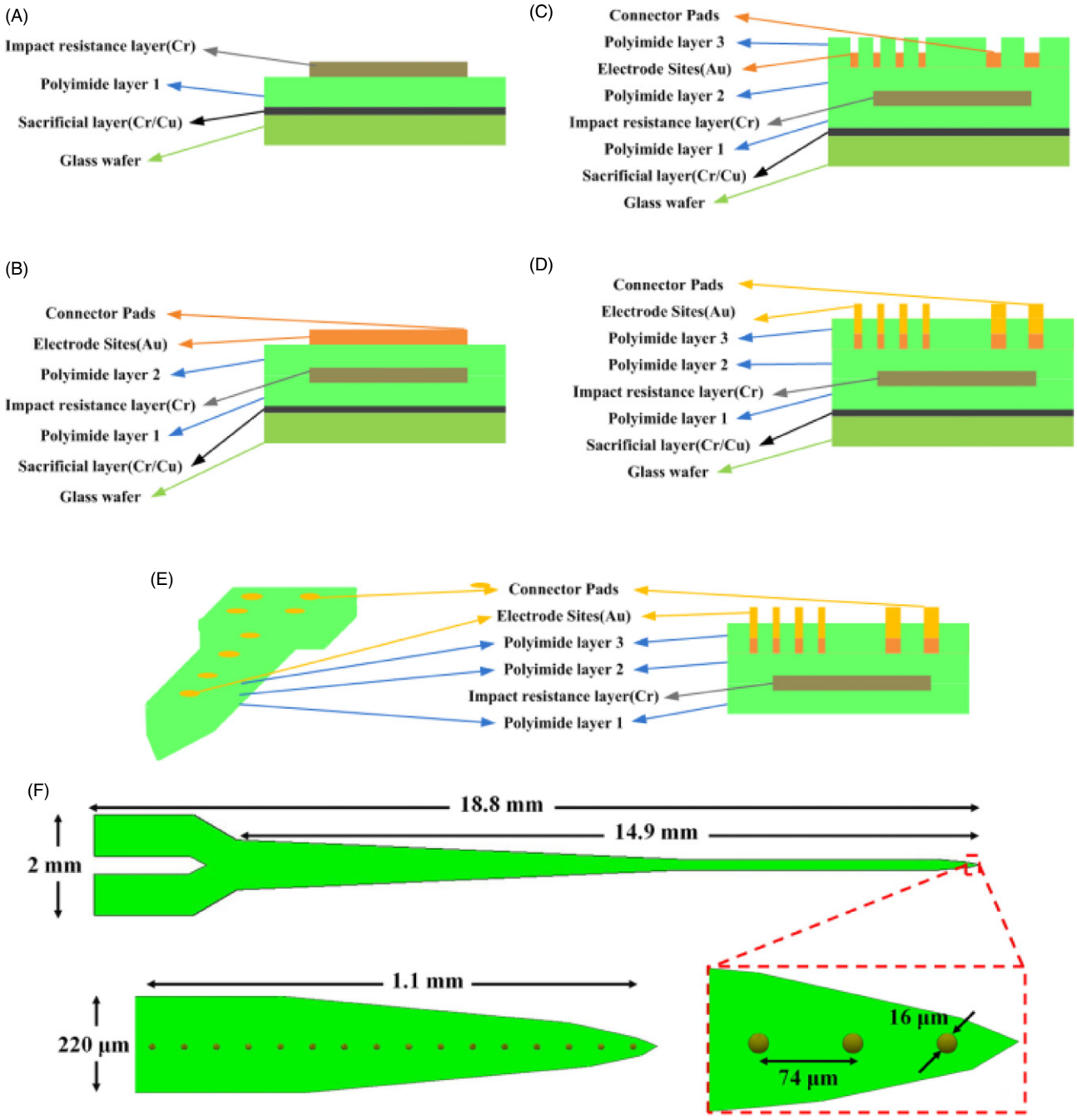

Figure 1. Fabrication process flow diagram and schematic view of the flexible neural probe.

2.3. FEM of thalamic stimulation

To investigate the effects of extracellular stimulation using different stimulation sets, 3D models of thalamic stimulation were implemented using FEM; the VTA was predicted using a multi-compartment cable model of a thalamocortical (TC) relay neuron (McIntyre *et al* 2004a, Rattay 1986, 1989, Warman *et al* 1992). The simulation processes in this study involved the following steps: (1) an axisymmetric FEM of the neural probe and brain tissue was created; (2) the stimulus current was applied to the electrode of the laboratory-designed neural probe, which was positioned in a homogeneous and isotropic volume conductor; (3) the potential distribution in the tissue medium was calculated using an FEM solver; and (4) the VTA was estimated using the ET within the TC relay neuron model.

A 3D FEM of the probe with 12 519 279 nodes was constructed using the commercially available software package ElecNet 7 (Infolytica Corp., Canada). The axisymmetric volume conductor surrounding the electrodes was modeled as a 1 mm^3 cube of homogeneous and isotropic tissue medium. The electrical resistivity of the gold electrode and the polyimide substrate of the laboratory-designed neural probe were 2.2×10^{-8} and 1.55×10^{16} Ω m, respectively. To comprehend the influence of tissue conductivity, neural probe stimulation models were implemented for the brain tissue

using an electrical conductivity of 0.1 (Butson and McIntyre 2008), 0.2 (Butson and McIntyre 2008, Wei and Grill 2005), 0.3 (McIntyre *et al* 2004a, Yaeli *et al* 2009) and 0.4 S m^{-1}. The distribution of the extracellular potential (V_e) generated in the tissue medium was calculated using a frontal solution method (McIntyre and Grill 2001, 2002, McIntyre *et al* 2004a) for the Laplace equation:

$$\nabla^2 V_e = 0. \quad (1)$$

The Laplace equation describes the potential variation in the electrolytic solution or tissue when the concentrations are uniform (Newman 1966). The extracellular potential was calculated using an FEM solver, and then the VTA was estimated using the ET within the TC relay neuron model (please refer to the appendix for details).

2.4. Animal preparation and grouping

In total, 30 male Wistar rats weighing 250–300 g (BioLASCO Taiwan Corp., Ltd) were used in the electrophysiological experiment. All procedures for the animal experiments were in accordance with the Guidelines for Care and Use of Experimental Animals outlined by the Laboratory Animal Center at National Chiao Tung University and National Yang Ming University.

The laboratory-designed neural probe was examined for its performance in chronic conscious recording, chronic stimulation recording, and c-*Fos* immunoreactivity mapping. For chronic neural activity recording, neural probes were implanted into five rats for neural activity recordings for a 50 day period. The quality of the recorded signals was evaluated with the SNR. For chronic stimulation recording, neural probes were implanted into five rats to record somatosensory evoked potentials (SSEPs) induced by thalamic stimuli for 50 days. This method was used to evaluate the SSEP changes in response to long-term stimulation. The remaining animals ($n = 20$) were used to investigate the magnitude of the changes in the c-*Fos* expression in rat brains elicited by activated volumes at intensities of 50, 100, 200 and 300 μA.

2.5. Chronic neural activity recording (n = 5)

Each rat was anesthetized with pentobarbital (50 mg kg^{-1} i.p.) and placed on a standard stereotaxic apparatus (Model 900, David Kopf, USA). After the dura was removed from the brain, the neural probe was inserted vertically into the right ventroposterior thalamus (VP, including ventral posteriomedial/posteriolateral nucleus (VPM/VPL)) with a target location of P 3 mm and L 3 mm with respect to the bregma and positioned 6 mm from the surface of the brain (Paxinos and Watson 2007). A stainless steel screw used as the reference electrode was positioned 2 mm caudal to lambda. The neural probe and the reference screw were permanently cemented to the bone using dental acrylic (Type 1 Class 1, Hygenic Corp., USA). During neural implantation and recording, the animals' blood pressure was maintained at >95 mmHg using a 3–4.5% end tidal CO_2 concentration. The rectal temperature was measured with a thermocouple and maintained at 37 ± 0.5 °C through a feedback-controlled blanked system (Harvard Apparatus, Holliston, Massachusetts, USA). After a one-week post-surgery recovery period, neural signals were recorded every two days for 50 days.

A multichannel acquisition processor (Plexon Inc., USA) was used to record neural signals from the 16-channel neural probe. During each recording session, the rat was free to move in the recording booth for 3 h; neural signals were recorded continuously for the last 30 min. The recorded signals were transmitted from the headstage to an amplifier through a band-pass filter (spike preamp filter: 450 Hz–5 kHz; gain: 15 000–20 000) and sampled at 40 kHz per channel. An automatic spike sorting tool (Lai *et al* 2011) was used to classify neural spikes recorded from each electrode on the neural probe. The quality of neural signals recorded was analyzed offline with the SNR estimation in MATLAB (MATLAB R11, Mathworks Inc., USA). The SNR of the neural signal was defined as the average peak-to-peak amplitude of spikes to the root mean square of the background noise (Ludwig *et al* 2006, Maynard *et al* 2000).

2.6. Chronic SSEP recording and in vivo electrode impedance measurement (n = 5)

Under isoflurane (Hospira, Lake Forest, Illinois, USA) anesthesia (induction 4%; maintenance 1.5%), the rats were placed on a standard stereotaxic apparatus (Model 900, David Kopf, USA). Two craniotomies were performed; epidural cortical electrodes were secured in the skull over the bilateral S1FL cortex (coordinates from bregma: AP, +0.5 mm; ML, ±4 mm) for electrocorticography (ECoG) recordings. A stainless steel screw used as the reference electrode was positioned 2 mm caudal to lambda. The two epidural cortical electrodes and the reference screw were permanently cemented to the bone using dental acrylic (Type 1 Class 1, Hygenic Corp., USA). For chronic thalamic stimulation, another craniotomy was performed for the implantation of the neural probe into the thalamic VPM/VPL (3 mm caudal to bregma, 3 mm from midline and 6 mm ventral to the pia surface). The neural probe was secured in the skull using dental acrylic and was covered with a small amount of 2% Agar. During neural implantation and recording, the animals' blood pressure was maintained at >95 mmHg using a 3–4.5% end tidal CO_2 concentration. The rectal temperature was measured with a thermocouple and maintained at 37 ± 0.5 °C through a feedback-controlled blanked system (Harvard Apparatus, Holliston, Massachusetts, USA).

Following a one-week recovery period, a biphasic constant current at 50, 100, 200 and 300 μA pulses, with a width of 0.3 ms at a frequency of 1 Hz, was administered using a stimulator (Model 2100, A-M Systems, USA) to each anesthetized rat (isoflurane induction 4%; maintenance 1.5%) receiving thalamic stimuli. The thalamic stimuli were administered between electrode sites #1 and #4 on the neural probe, with a fixed distance of 198 μm. Meanwhile, bilateral SSEPs were filtered on pre-amp between 0.3 and 500 Hz and sampled at 1 kHz; data acquisition was performed using a Cerebus multichannel data

acquisition system (Blackrock Microsystems, Salt Lake City, Utah, USA). The SSEP recording was performed every two days for 50 days; each stimulus intensity was presented once to each animal.

The SSEPs were analyzed offline using MATLAB (MATLAB R12, Mathworks Inc., USA) to evaluate the evoked responses induced by thalamic electrical stimuli. The evoked SSEP amplitudes of individual sweeps were averaged over 150 sweeps to generate an averaged evoked SSEP. Afterwards, the averaged evoked SSEP was summed to obtain an absolute value of the amplitudes for the evoked response during the 200 ms post-stimulus period, denoted as ΣSSEP. ΣSSEP changes were used to evaluate the stabilities of the evoked responses induced by the thalamic stimuli over long periods. Furthermore, the coefficient of determination (R^2) of the linear curve fit was statistically evaluated from the relationship between the ΣSSEP and the stimulus intensities of 50, 100, 200 and 300 μA.

The *in vivo* electrode–electrolyte interface impedance was measured in animals with implants every two days for 50 days after the one-week recovery period. The impedance of the 16 implanted electrodes was measured using a sinusoidal voltage source (20 mV, <150 nA, at 1 kHz) through electrode sites #1 and #4. The impedance measurement method was based on the standard method adopted in previous studies (Chang and Chiou 2010, Chen *et al* 2009).

2.7. C-Fos immunohistochemistry mapping (n = 20)

In total, 20 animals with thalamic implantation (similar to the procedures described in section 2.6) were divided into four groups (five per group). The animals received 1 Hz thalamic stimulation at 50, 100, 200 and 300 μA for 150 s. The animals were sacrificed 2 h after thalamic stimulation, as this delay corresponds to the maximum c-*Fos* expression after a variety of stimulation situations (Herrera and Robertson 1996). Each rat was anesthetized with an overdose of pentobarbital solution (50 mg kg^{-1} i.p.) and then perfused with 300 ml of 0.05% heparin in PBS and 300 ml of 4% paraformaldehyde (PFA) in PBS at a flow rate of 15 ml min^{-1}. The brain was carefully extracted from the skull and soaked in a mixture of 4% PFA and 30% sucrose at 4 °C for 2 h, upon which the brain was soaked in PBS. Each brain was sliced into 50 μm coronal sections with a freezing microtome (object temperature = −15 °C, CM 1800, Leica, Germany).

The brain slices were washed in PBS (3 × 10 min) and placed in 0.1% H_2O_2 in PBS for 60 min before being washed in PBS (3 × 10 min). Following placement in 10% bovine serum albumin for 2 h, the slices were washed again in PBS (3 × 10 min). The slices were incubated with a polyclonal rabbit anti c-*Fos* antibody (Novus Biologicals, LLC, USA) at dilutions of 1:300 in PBS for 16 h at 4 °C. Subsequently, the slices were washed in PBS (3 × 10 min) and incubated with anti-rabbit IgG biotin conjugate (Novus Biologicals, LLC, USA) at dilutions of 1:300 in PBS for 1.5 h.

After washing in PBS (3 × 10 min), the slices were incubated in an avidin–biotin complex (ABC, Wako Pure Chemical Industries, Ltd, Japan) solution at dilutions of 1:100 for 60 min. The slices were then washed in 0.05 M Tris-HCl buffer (Wako Pure Chemical Industries, Ltd, Japan) (3 × 10 min) and immersed in a mixture solution of 0.05% 3′-3′-diaminobenzidine (Wako Pure Chemical Industries, Ltd, Japan) and 0.1% H_2O_2 (10 min). Then, the slices were washed in 0.05 M Tris-HCl buffer (3 × 10 min). Each slice was eluted in an ethanol gradient (75% ethanol, 85% ethanol, 90% ethanol, 95% ethanol and 99.9% ethanol) for 3 min and dehydrated in xylene (Fullin Nihon Shiyaku Bio., Ltd, Taiwan) for 10 min. Finally, each slice was dried and placed in a Permount medium for further optical microscopic image observations and analysis.

The quantification of c-*Fos* positive immunoreactivity within the thalamic nucleus was performed bilaterally for 30 slices ranging from 2.2–3.7 mm posterior to the bregma for each rat for each selected brain region using freeware Image Processing and Analysis in Java (ImageJ, NIH). Cell counts per mm^2 were analyzed for the bilateral central lateral (CL), VP and mediodorsal (MD) nucleus of the thalamus (Paxinos and Watson 2007). A linear data fit with a corresponding coefficient of determination (R^2) was used to determine the relationship between the positive c-*Fos* expression in the thalamus and the activated volumes produced by the stimulus intensities of 50, 100, 200 and 300 μA. The higher the R^2 value for the activated volumes, the more sensitive the positive c-*Fos* expression is to that of the stimulus intensities. R^2 values of above 0.8 indicate a statistically good fit.

The resulting mean values and standard deviation (mean ± SD) for the data, including *in vivo* impedance, SNR, ΣSSEP, *in vivo* electrode–electrolyte interface impedance and c-*Fos* positive nuclei, are presented in the text.

3. Results

3.1. Assembly of the neural probe

The neural probe was designed for both implantation and long-term recording and was constructed as depicted in figure 2(A). The neural probe was bonded onto a miniature printed circuit board, which was combined with a connector (A8141-001, Omnetics Connector Corp., USA). Because of its small size and lightness (<3 g), the neural probe can be implanted into the rat brain while permitting relative free movement for the animal. In figure 2(B), the 16 electrode sites and interconnecting traces located on the long shaft of the polyimide substrate are shown. A rough 3D microstructure of the electrode surface obtained by scanning electron microscopy (SEM) is presented in figure 2(C). The flexibility of the probe is demonstrated by its capability of returning to its original shape even after being bent (figure 2(D)). The Young modulus, a measure of the stiffness of an isotropic elastic material (Cheung 2007, Subbaroyan *et al* 2005), of the laboratory-designed neural probe was approximately 54 GPa.

3.2. Effective areas of electrical stimulation

The primary goal of this FEM simulation was to characterize the spread of electrical stimulation in the brain tissue following DBS. The effects of the stimulus intensity were quantified

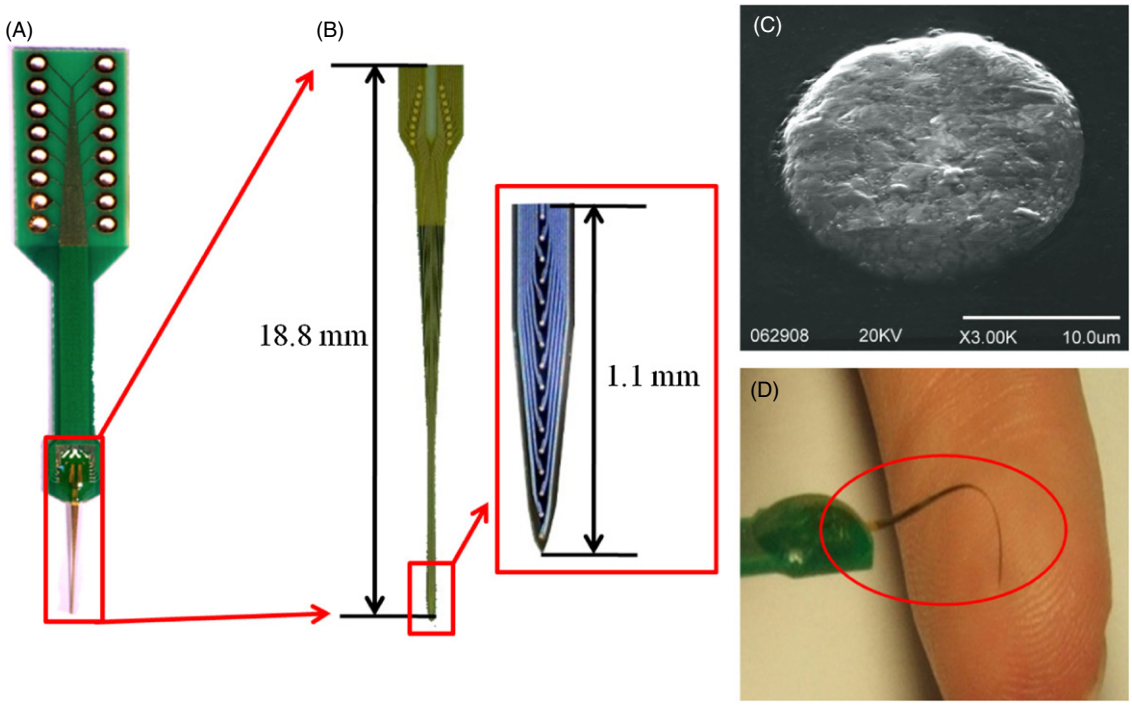

Figure 2. (A) An overall view of the laboratory-designed neural probe, (B) specifications of the neural probe, (C) SEM image of the electrode surface and (D) demonstration of the flexibility of the neural probe.

by calculating the VTA. The extracellular potential (V_e) distributions generated from bipolar stimulation at different intensities in homogeneous and isotropic tissue with a conductivity of 0.3 S m^{-1} are shown in figure 3. Upon the administration of currents of 50, 100, 200 and 300 μA, the voltage values at the surface of electrode site #1 were 4.4216, 8.8432, 17.6864 and 26.5296 V, respectively. The potential distribution increased as the current stimulus was increased. The VTA values at various stimulus intensities for parallel fibers are shown in figure 4. When current stimuli of 50, 100, 200 and 300 μA were administered to tissue with a conductivity of 0.3 S m^{-1}, the VTA values were 9625, 17 250, 32 625 and 44 125 μm^3, respectively. Therefore, the VTA values were found to increase with the stimulation intensities. The VTA values for parallel fibers in tissues with different conductivities are shown in figure 5. The VTA values for all tissue conductivities were extended with increased stimulus intensity. In addition, the VTA values increased with the tissue conductivity for each current stimulus level.

3.3. The quality of chronic neural recordings

Because minimizing the electrode impedance is an important requirement for obtaining high-quality neural recordings, electrodes with rough 3D structure were fabricated by the electroplating processing in this study. The average *in vitro* impedance of the five neural probes was 2.60 $\pm$ 0.52 MΩ at 1 kHz (mean $\pm$ SD, $n = 5$), which worked reasonably well in acute and chronic implanted applications.

As the neural probe was primarily designed for long-term recording, the quality of chronic neural recording was also evaluated. A freely moving rat with the implanted neural probe was placed in the recording booth, as shown in figure 6(A). A photomicrograph of the implantation section is shown in figure 6(B). The figure was modified by superimposing one lesion marker on one implantation track, which was then overlaid with a scaled image of the designed probe. The lesion marker was used to identify the location of the outermost recording site. The spontaneous neural activities simultaneously recorded from the 16 electrodes are shown in figure 6(C).

After implantation, the SNRs of the implanted neural probe were measured. The SNR was 4.87 $\pm$ 0.40 and 4.72 $\pm$ 0.34 (mean $\pm$ SD, $n = 5$) on day 0 and day 50, respectively. The SNR of the recorded signals ranged from 4.4 to 5, with no significant decrease throughout the experimental session (p-value $= 0.103$; repeated measures ANOVA; $n = 5$), as shown in figure 6(D). These results illustrate the stability and high quality of long-term recordings performed using the laboratory-designed neural probe.

3.4. The stability of SSEPs and in vivo electrode–electrolyte interface impedance for long-term stimuli

An example of the averaged SSEPs on days 0 and 50 is shown in figure 7(A). Increased intensities of thalamic stimuli resulted in increased SSEP magnitudes. Insignificant differences in SSEP morphology were observed between day 0 and day 50 under the same intensity of thalamic stimuli. The chronic change in ΣSSEP was used to evaluate the stability of the long-term stimuli in the thalamic VP, as shown in figure 7(B). The 50 day averaged ΣSSEPs for 50, 100, 200 and 300 μA thalamic stimuli were 7.83 $\pm$ 0.54, 8.85 $\pm$ 0.61, 11.15 $\pm$ 0.68 and 16.72 $\pm$ 0.55 mV/200 ms, respectively. The results indicate that no significant variance in ΣSSEP is observed over time (p-value $= 0.156$; repeated measures

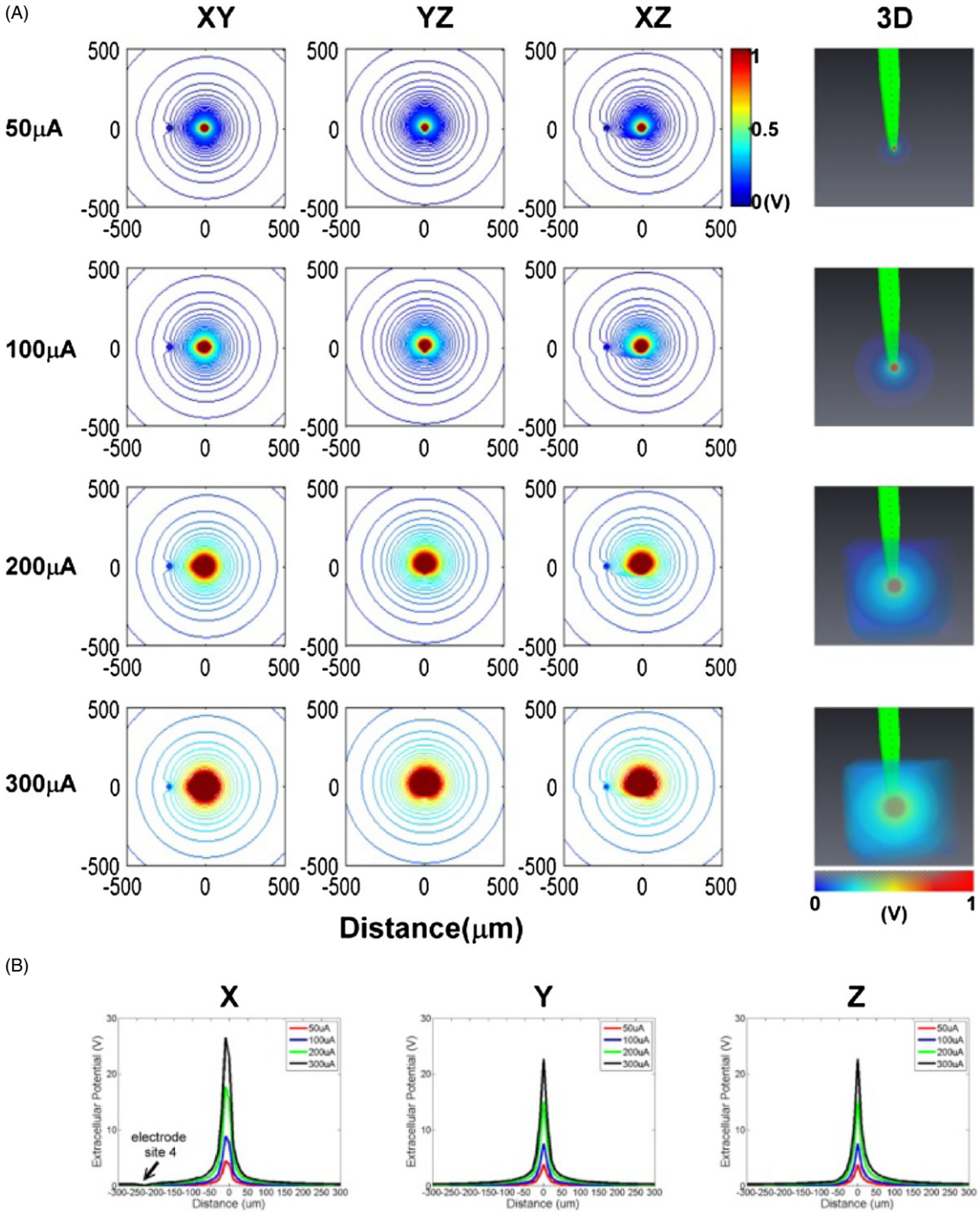

Figure 3. The effects of stimulus intensity on the extracellular potential. (A) Two-dimensional and (B) one-dimensional distributions of the extracellular potential generated by bipolar stimulation in tissue with a conductivity of 0.3 S m^{-1} at various stimulus intensities (50, 100, 200 and 300 μA).

ANOVA; $n = 5$). The *in vivo* electrode–electrolyte interface impedance (at 1 kHz) was measured to detect chronic tissue proliferation around the electrodes (Suner *et al* 2005). After implantation (day 0), the laboratory-designed probe's *in vivo* electrode–electrolyte interface impedance (at 1 kHz) was 0.25 $\pm$ 0.06 MΩ (mean $\pm$ SD, $n =$ 20). During the 50 days after implantation, the variation of the *in vivo* electrode–electrolyte interface impedance was small, with similar impedance values of 0.25 $\pm$ 0.06 and 0.24 $\pm$ 0.05 MΩ recorded on day 14 and day 50, respectively. No significant change in the *in vivo* electrode–electrolyte interface impedance was observed during the chronic stimulation session (p-value $=$ 0.114; repeated measures ANOVA; $n = 5$), as demonstrated in figure 7(C). The relationship between the ΣSSEP results and stimulus intensities was also examined. The black line in figure 7(C)

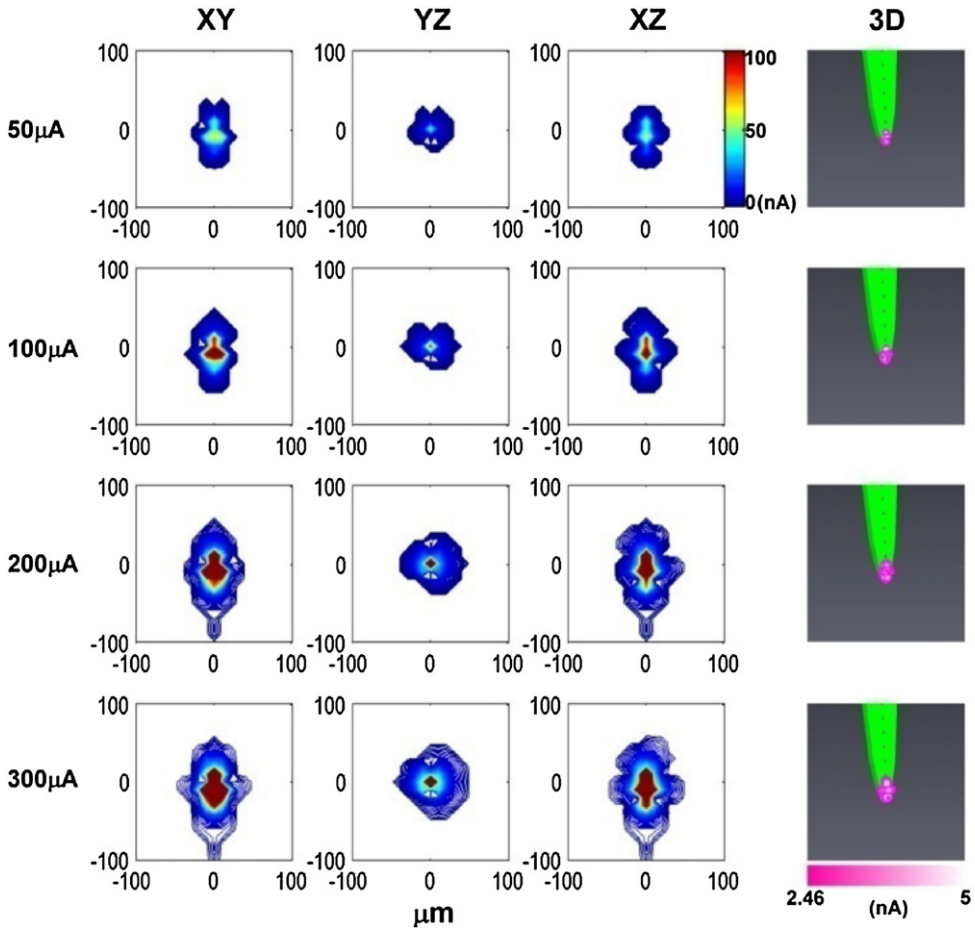

Figure 4. The effects of the stimulus intensity on the VTA. The VTA values obtained from bipolar stimulation at various stimulus intensities (50, 100, 200 and 300 μA) are shown when the fiber is parallel to the shaft of the neural probe. VTA activation increases as the stimulus intensity increases.

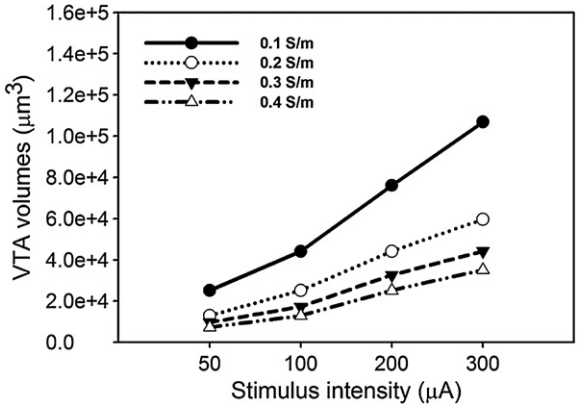

Figure 5. The effects of the stimulus intensity on the VTA for different tissue conductivities. The VTA values increase with increased stimulus intensity for various tissue conductivities.

represents the linear curve fit ($R^2 = 0.9927$). The results suggest a significantly linear relationship between the ΣSSEP results and the stimulus intensities. The value of the slope is close to 1 (slope = 0.9927), suggesting that the stimulus intensities were almost perfect in predicting the evoked responses (SSEP).

3.5. C-Fos expression induced by thalamic stimuli

The quantification of c-*Fos* immunoreactivity within bilateral thalamic nuclei induced by thalamic stimuli is presented in table 1. For the thalamic nuclei of the CL, VP and MD, increased numbers of cell clusters immunoreactive to c-*Fos* were observed with increased stimulus intensities, as shown in figure 8(A). The ipsilateral thalamic CL and VP nuclei exhibited a significantly higher number of c-*Fos*-labeled cells compared with their contralateral counterparts (p-value $<$ 0.05; Student's t-test; $n = 20$).

Figure 8(B) presents the correlation test between the summation of the number of c-*Fos*-labeled cells in the thalamic CL, VP and MD nuclei and stimulus intensities. The strong linear fit has coefficients of determination (R^2) of 0.9704 and 0.9574 for the ipsilateral and contralateral sides in the thalamus, respectively.

3.6. Linear relationship among VTA predications, in vivo SSEPs and c-Fos expressions

The linear curve fit between ΣSSEP and the c-*Fos* expression is shown in figure 9(A). The coefficient of determination (R^2) between the ΣSSEP and the c-*Fos* expression was 0.9482. The significantly linear relationship indicates that the two

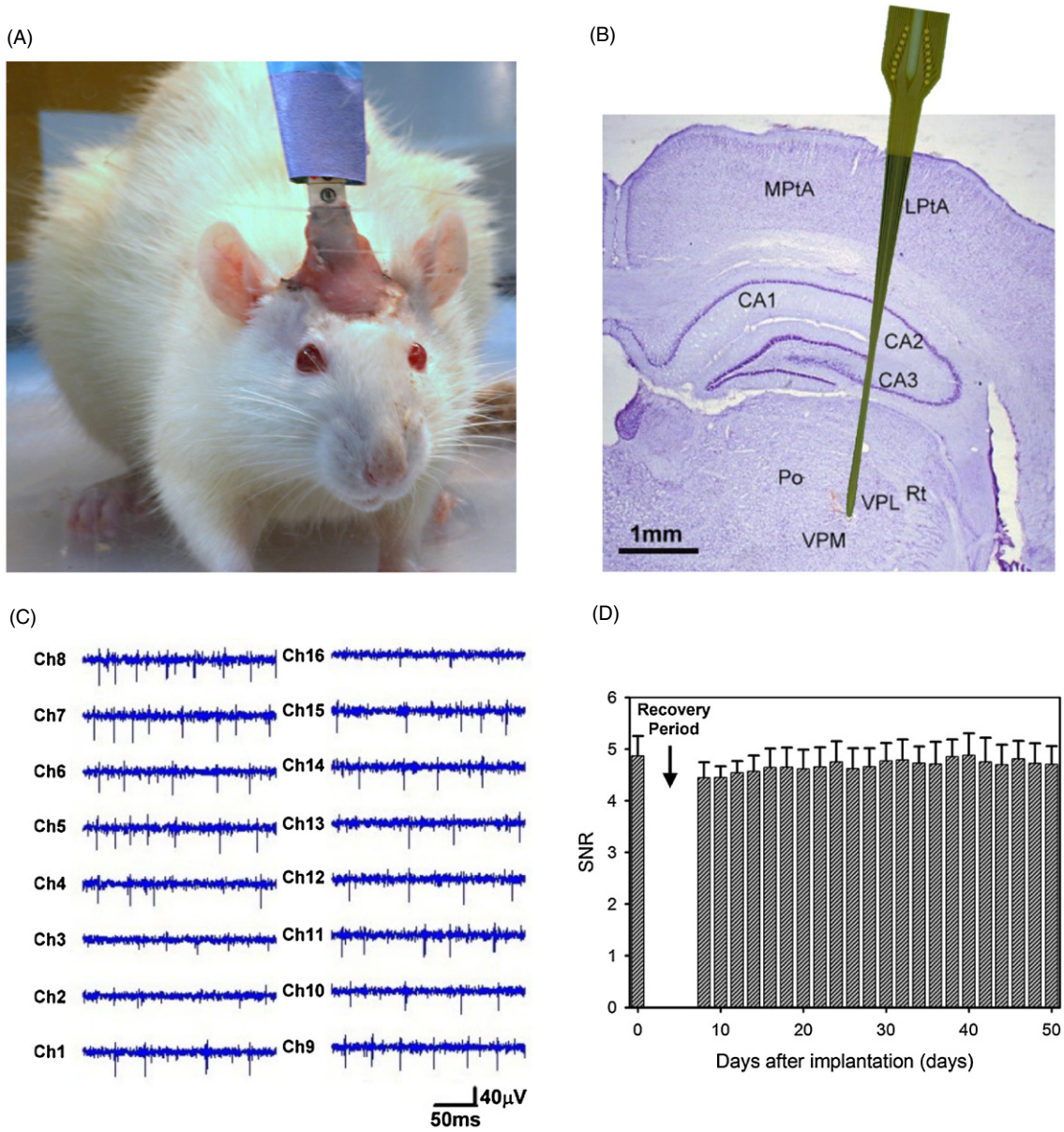

Figure 6. (A) A photograph of a rat implanted with the laboratory-designed neural probe. The rat was free to move around in the recording booth. (B) The photomicrograph of a Nissl-stained coronal section at 3 mm posterior to bregma. The *in situ* location of the neural probe is also shown. Po: the posterior thalamus nuclear group; Rt: reticular thalamus nucleus; VPM: ventral posteromedial thalamus nucleus; VPL: ventral posterolateral thalamic nucleus. (C) An example of the 16-channel neural activity simultaneously recorded from the right VP thalamus of a freely moving rat using the laboratory-designed neural probe on day 50. (D) The mean SNR of the recording signals averaged for five rats across the recording session.

Table 1. Cell counts mm^{-2} for c-*Fos* in thalamus.

	50 μA		100 μA		200 μA		300 μA	
Thalamic nuclei	Ipsilateral	Contralateral	Ipsilateral	Contralateral	Ipsilateral	Contralateral	Ipsilateral	Contralateral
CL*	143 ± 52	122 ± 64	303 ± 14	3279 ± 27	441 ± 16	378 ± 13	528 ± 36	408 ± 33
VP*	226 ± 29	198 ± 42	428 ± 52	381 ± 24	533 ± 53	427 ± 60	592 ± 70	487 ± 54
MD	123 ± 24	118 ± 32	202 ± 66	207 ± 49	511 ± 40	521 ± 56	719 ± 58	722 ± 58

CL: central lateral nucleus of the thalamus; VP: ventroposterior nucleus of the thalamus; MD: mediodorsal nucleus of the thalamus. The right hemisphere of thalamic stimulation: ipsi- or contralateral to the neural probe placement.
* p-value <0.05: statistically significant differences between bilateral thalamic nuclei.
(Mean ± SD.)

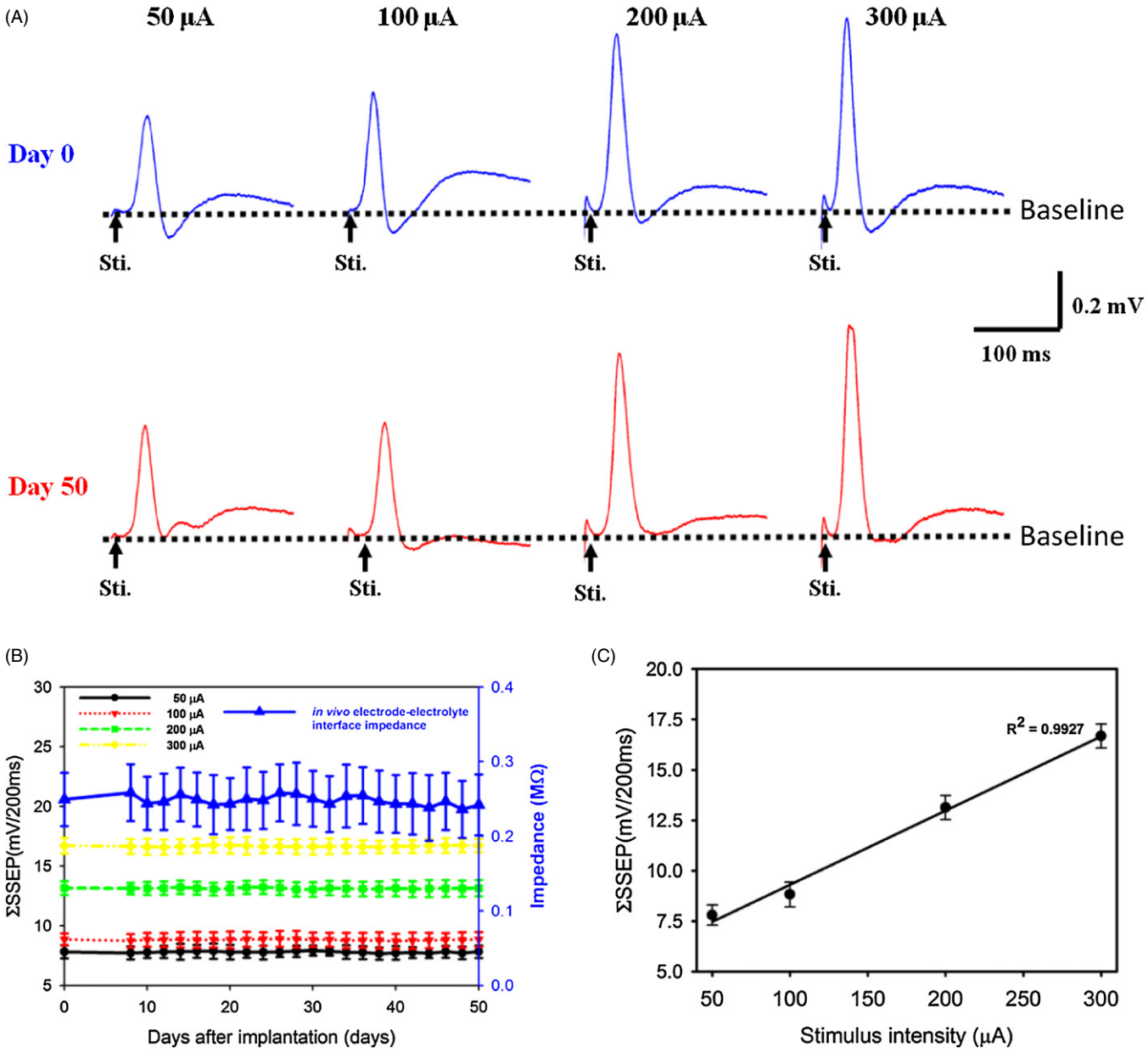

Figure 7. (A) The SSEP morphologies obtained from ECoG with different stimulus intensities (50, 100, 200 and 300 μA). The responses were averaged across 150 repetitions on day 0 and day 50. The arrowheads indicate the stimulating moments for each stimulus intensity. (B) The ΣSSEP with different stimulus intensities recorded from five rats during the thalamic stimulation session. The blue line presents the *in vivo* electrode–electrolyte interface impedance over the stimulation session. (C) The mean ΣSSEP averaged from the 50 day ECoG recordings obtained from five rats with different stimulus intensities. The linear curve fit shows a strong correlation ($R^2 = 0.9927$) between the ΣSSEP and the stimulus intensity.

experiments produced similar results. Figure 9(B) shows the linear curve fit between ΣSSEP and the VTA values for tissue conductivities of 0.1 (black line), 0.2 (red line), 0.3 (green line) and 0.4 (yellow line) S m^{-1}. The optimal fit ($R^2 = 0.9781$) between ΣSSEP and VTA was obtained for a tissue conductivity of 0.2 S m^{-1} (red line). The correlation between the c-*Fos* expression and the VTA values at different tissue conductivities is shown in figure 9(C). The optimal coefficient of determination ($R^2 = 0.9923$) between the c-*Fos* expression and VTA was obtained for a tissue conductivity of 0.2 S m^{-1}. These results indicate an ideal sensitivity to predict evoked responses (c-*Fos* expression) based on the VTA. Therefore, significantly linear relationships exist among the VTA, ΣSSEP and c-*Fos* expression level.

4. Discussion

In this study, a novel flexible microelectrode neural probe was designed, fabricated and validated experimentally through *in vitro* and *in vivo* characterization of its performance during stimulation and recording applications. Metallic layers were sandwiched between polyimide layers to strengthen the neural probe to withstand insertion forces and to allow accurate positioning of the tip at the target of interest. In addition, electroplating was used to increase the sturdiness,

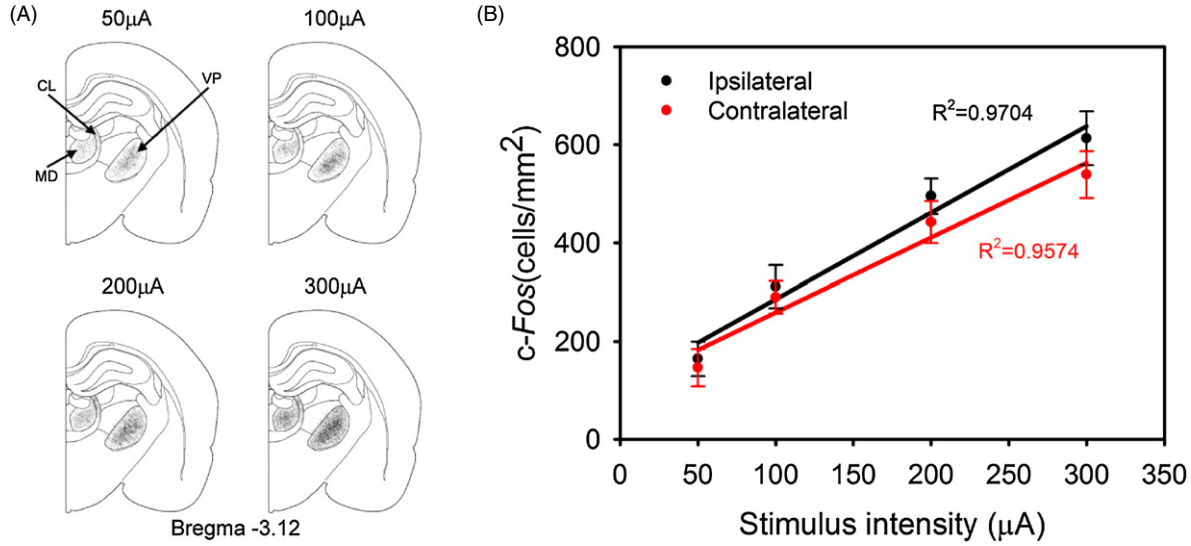

Figure 8. (A) An example of the topographic organization of the ipsilateral CL, VP and MD nucleus of the thalamus (slice location: 3.12 mm posterior to the bregma) for different stimulus intensities (50, 100, 200 and 300 μA). (B) The c-*Fos* expression levels were counted within the bilateral CL, VP and MD nucleus of the thalamus from 30 brain slices (2.2 to 3.7 mm posterior to the bregma) of each rat. The black line representing the linear curve fit between the number of ipsilateral c-*Fos* positive nuclei and the stimulus intensities shows a strong correlation ($R^2 = 0.9704$). The red line representing the linear curve fit between the number of contralateral c-*Fos* positive nuclei and the stimulus intensities also shows a strong correlation ($R^2 = 0.9574$) ($n = 5$ for each stimulus intensity).

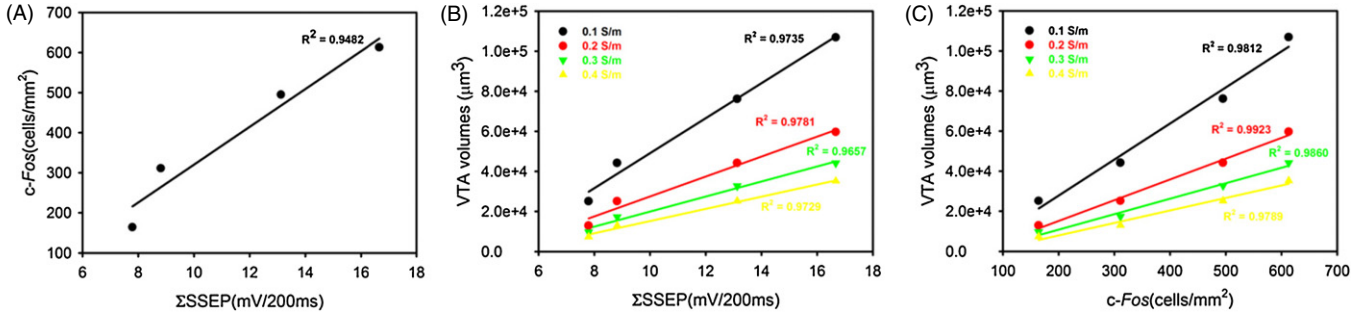

Figure 9. (A) The linear curve fit between the ΣSSEP and number of bilateral c-*Fos* positive nuclei shows a positive correlation ($R^2 = 0.9482$). (B) The black, red, green and yellow lines represent the linear curve fit for tissue conductivities of 0.1, 0.2, 0.3 and 0.4 S m^{-1}, respectively. The optimal correlation ($R^2 = 0.9781$) between the ΣSSEP and the VTA was obtained for 0.2 S m^{-1} tissue conductivity. (C) The black, red, green, and yellow color lines represent the linear curve fitting results for tissue conductivities of 0.1, 0.2, 0.3 and 0.4 S m^{-1}, respectively. The optimal coefficient of determination ($R^2 = 0.9923$) between the ipsilateral c-*Fos* expression and the VTA was obtained at 0.2 S m^{-1} tissue conductivity.

density and thickness of each electrode, thus extending the lifespan for signal recordings and electrolytic stimulation. The SNR and ΣSSEP results indicate that the neural probe is feasible for long-term recording and stimulation. Furthermore, the mechanisms and factors affecting the DBS outcome were evaluated using VTA estimation. A strongly positive correlation exists among the VTA estimation value, ΣSSEP and c-*Fos* expression value.

Due to its smaller Young modulus, a probe with 'soft' substrate may bend substantially near the brain surface (Subbaroyan *et al* 2005). Durable materials are required to construct a microelectrode array that is stiff enough to withstand insertion forces and long enough to penetrate into the subcortical brain without bending or path deviation to ensure accurate electrode placement. An impact resistance layer constructed by sandwiching a 200 nm thick chrome layer between two 30 μm thick polyimide layers was applied to the laboratory-designed probe. This design increased the strength of the polyimide-based microelectrode array while retaining its flexibility. The Young modulus of the laboratory-designed probe was increased to 54 GPa, within the range of the Young modulus of silicon-based microelectrode arrays (∼170 GPa) and purely polyimide-based microelectrode arrays (∼3 GPa). Therefore, the harmful effects caused by micromotion (Cheung 2007, Kim *et al* 2004, Ludwig *et al* 2006), including protein adsorption, macrophage fusion to the electrode and the development of an encapsulation layer around the tissue–electrode contact area, were reduced, and the stability for chronic recordings was improved. The SNR estimation results of the laboratory-designed probe recording ranged from 4 to 5 over the course of the 50 day recording period, demonstrating that the signals were of good quality (Ludwig *et al* 2006). In addition, the SNR variation of the laboratory-designed probe was smaller than that of Ludwig *et al* (2006). The SNR of the recorded signals remained stable and

qualitative, implying that the laboratory-designed probe was stable and reliable enough for long-term recording.

The probe specifically designed for stimulation contains a gold metal trace with a lower resistivity to provide for lower voltage drops during stimulation current passage. Our evaluations indicated that the *in vivo* electrode–electrolyte interface impedances of the electroplated Au electrodes on the probe were smaller than those of the thin-film-deposited electrodes on a commercial probe. In addition, the electroplating process produced harder, denser and thicker electrodes that could withstand a large amount of metal dissolution (De Haro *et al* 2002). Hence, the electroplated Au electrodes on the laboratory-designed neural probe could tolerate stronger electrical conduction than the thin-film-deposited electrodes on the silicon-based probe (Chen *et al* 2009).

The electroplating process produced Au electrodes with rougher surfaces according to SEM evaluations, thus increasing the effective surface area and reducing the electrode impedance (De Haro *et al* 2002, Kovacs 1994, Paik *et al* 2003, Heim *et al* 2011). In addition, these rougher surfaces provided an increased surface area, resulting in a significantly increased double layer capacitance that was mostly polarizable and included an interface impedance that was mostly represented by capacitance (Butson and McIntyre 2005). An electrode with high polarization can accommodate a large amount of charge on the double layer and is therefore desirable for stimulation (Butson and McIntyre 2005, Wei and Grill 2009). The quantitative measurements of the *in vivo* electrode–electrolyte interface impedance demonstrated an increased impedance magnitude on day 8. After this initial increase, the impedance remained constant for the next week until the end of the experiment. Moreover, the SSEP in S1FL induced by thalamic stimuli maintained a consistent magnitude in the evoked response over the 50 day experimental period. Therefore, the electroplating process produced Au electrodes with an improved stability for charge delivering capacity, which is a requirement for chronic applications.

Studies have applied simulated models using FEM analysis to predict VTA changes in the human brain (Butson and McIntyre 2008, Stamatios and Peter 2007, Butson and McIntyre 2006). Due to the limitations of human experiments, the first animal study was performed to compare the predicted VTA changes and real neural responses with the same electrode placement and stimulation parameter settings. Here, the stimulated area in the thalamus was small; therefore, the tissue conductivity was homogeneous across various depths (Anderson *et al* 1989, Townsend *et al* 2002), especially in the complex VP nuclei in the rodent model (Emmers 1988, Chen *et al* 2004). Furthermore, the laboratory-designed probe with a small electrode size provided precise stimulation to induce specific SSEP changes in the cortical area and c-*Fos* expression in the thalamic VP nuclei. The simulated VTA results demonstrated excellent correlation ($R^2 > 0.96$) with SSEP changes and the c-*Fos* expression value, which indicated that simulated VTA during thalamic stimuli can characterize the sensitivity of the neural responses. Although VTA prediction using FEM with the homogeneous and isotropic medium may be reliable in the rodent model, the predictions may not be as accurate in humans (Butson and McIntyre 2005, 2006). Possible reasons for this difference are as follows. (1) The diameter of the myelinated axon of TC relay neurons in the human brain is larger than that in the rat brain. (2) All nodes of Ranvier along the fibers were set in the same direction in our FEM simulation. However, more random fiber directions relative to the electrode may reduce the VTA (Butson and McIntyre 2006), and (3) to focus on the single impact of stimulation intensity, the effects of fiber direction, electrode configuration, and inhomogeneous and anisotropic tissue medium were not discussed here (Butson and McIntyre 2005, 2006).

Acknowledgments

This work was supported in part by the UST-UCSD International Center of Excellence in Advanced Bioengineering and sponsored by the Taiwan National Science Council I-RiCE Program under grant number NSC-100-2911-I-009-101. This work was also supported in part by the Aiming for the Top University Plan of National Chiao Tung University, the Ministry of Education, Taiwan, under grant number 100W9633, in part by the National Science Council, Taiwan, under contracts NSC-101-2622-E-010-002-CC2, NSC-100-2320-B-010-031-MY2, NSC-100-2628-E-010-004 and NSC-100-2321-B-009-003, and in part by the VGHUST Joint Research Program, Tsou's Foundation, Taiwan, under contract VGHUST101-G5-2-1. We would also like to thank 7 T animals MRI Core Lab of the Neurobiology and Cognitive Science Center for the technical and facility support and C-H Hsieh and J-H Chen of the Instrumentation Center for their assistance with the MRI experiments at National Taiwan University.

Appendix. Estimation of volumes of tissue activated

To understand the interaction between the electrode on the laboratory-designed probe and the neural tissue, the ET was used to predict the activation patterns of neurons by extracellular potentials (McIntyre *et al* 2004, Rattay 1989; Warman *et al* 1992). ETs are defined as the minimum voltage that generated action potentials at the soma, the dendrites and the myelinated axon. First, the AF, $f(n)$, was calculated from the extracellular potential (V_e) at each segment, n, as follows (Woock *et al* 2010):

$$\begin{aligned} f(n) &= \frac{\Delta^2 V_e}{\Delta x^2} \\ &= \frac{[V_e(n+1) - V_e(n)] - [V_e(n)] - V_e(n-1)}{L^2} \\ &= \frac{V_e(n-1) - 2V_e(n) + V_e(n+1)}{L^2}, \end{aligned} \tag{A.1}$$

where n is the node of interest and L is the internodal length. The activation patterns are related to the second spatial derivative of the extracellular potential along the axis of the nerve fiber (Rattay 1989, Warman *et al* 1992). Next, TC relay neuron models were implemented using NEURON v. 7.1 (Carnevale and Hines 2006) to estimate the ET at the

elements of the TC relay neuron (Butson and McIntyre 2005, 2006, Moffitt *et al* 2004, Stamatios and Peter 2007). An action potential occurs when the AF exceeds the ET. Finally, the VTA values can be predicted by calculating the volumes for which neuronal excitation occurs.

References

Anderson D J, Najafi K, Tanghe S J, Evans D A, Levy K L, Hetke J F, Xue X, Zappia J J and Wise K D 1989 Batch fabricated thin-film electrodes for stimulation of the central auditory system *IEEE Trans. Biomed. Eng.* **36** 693–704

Biran R, Martin D C and Tresco P A 2005 Neuronal cell loss accompanies the brain tissue response to chronically implanted silicon microelectrode arrays *Exp. Neurol.* **195** 115–26

Branner A and Normann R A 2000 A multielectrode array for intrafascicular recording and stimulation in sciatic nerve of cats *Brain Res.* **51** 293–306

Branner A, Stein R B, Fernandez E, Aoyagi Y and Normann R A 2004 Long-term stimulation and recording with a penetrating microelectrode array in cat sciatic nerve *IEEE Trans. Biomed. Eng.* **51** 146–57

Brozoski T J, Caspary D M and Bauer C A 2006 Marking multi-channel silicon-substrate electrode recording sites using radiofrequency lesions *J. Neurosci. Methods* **150** 185–91

Butson C R, Maks C B and McIntyre C C 2006 Sources and effects of electrode impedance during deep brain stimulation *Clin. Neurophysiol.* **117** 447–54

Butson C R and McIntyre C C 2005 Tissue and electrode capacitance reduce neural activation volumes during deep brain stimulation *Clin. Neurophysiol.* **116** 2490–500

Butson C R and McIntyre C C 2006 Role of electrode design on the volume of tissue activated during deep brain stimulation *J. Neural Eng.* **3** 1

Butson C R and McIntyre C C 2008 Current steering to control the volume of tissue activated during deep brain stimulation *Brain Stimul.* **1** 7–15

Carnevale N T and Hines M L 2006 *The Neuron Book* (Cambridge: Cambridge University Press)

Chang C-W and Chiou J-C 2010 Development of a three dimensional neural sensing device by a stacking method *Sensors* **10** 4238–52

Chen Y-Y, Lai H-Y, Lin S-H, Cho C-W, Chao W-H, Liao C-H, Tsang S, Chen Y-F and Lin S-Y 2009 Design and fabrication of a polyimide-based microelectrode array: application in neural recording and repeatable electrolytic lesion in rat brain *J. Neurosci. Methods* **182** 6–16

Chen Y Y, Kuo T S and Jaw F S 2004 A laser micromachined probe for recording multiple field potentials in the thalamus *J. Neurosci. Methods* **139** 99–109

Cheung K C 2007 Implantable microscale neural interfaces *Biomed. Microdevices* **9** 923–38

Cheung K C, Renaud P, Tanila H and Djupsund K 2007 Flexible polyimide microelectrode array for *in vivo* recordings and current source density analysis *Biosens. Bioelectron.* **22** 1783–90

De Haro C, Mas R, Abadal G, Munoz J, Perez-Murano F and Dominguez C 2002 Electrochemical platinum coatings for improving performance of implantable microelectrode arrays *Biomaterials* **23** 4515–21

Emmers R 1988 *Somesthetic System of The Rat* (New York: Raven)

Ensell G, Banks D J, Ewins D J, Balachandran W and Richards P R 1996 Silicon-based microelectrodes for neurophysiology fabricated using a gold metallization/nitride passivation system *J. Microelectromech. Syst.* **5** 117–21

Grill W and Thomas Mortimer J 1994 Electrical properties of implant encapsulation tissue *Ann. Biomed. Eng.* **22** 23–33

Haberler C, Alesch F, Mazal P R, Pilz P, Jellinger K, Pinter M M, Hainfellner J A and Budka H 2000 No tissue damage by chronic deep brain stimulation in Parkinson's disease *Ann. Neurol.* **48** 372–6

Hamani C, Nobrega J N and Lozano A M 2010 Deep brain stimulation in clinical practice and in animal models *Clin. Pharmacol. Ther.* **88** 559–62

Heim M, Yvert B and Kuhn A 2011 Nanostructuration strategies to enhance microelectrode array (MEA) performance for neuronal recording and stimulation *J. Physiol.* at press (doi:10.1016/j.jphysparis.2011.10.001)

Hemm S, Vayssiere N, Mennessier G, Cif L, Zanca M, Ravel P, Frerebeau P and Coubes P 2004 Evolution of brain impedance in dystonic patients treated by gpi electrical stimulation *Neuromodulation: Technol. Neural Interface* **7** 67–75

Herrera D G and Robertson H A 1996 Activation of c-fos in the brain *Prog. Neurobiol.* **50** 83–107

Johnson M D, Otto K J and Kipke D R 2005 Repeated voltage biasing improves unit recordings by reducing resistive tissue impedances *IEEE Trans. Rehabil. Eng.* **13** 160–5

Joseph J and Fins M F 2009 Deep brain stimulation, deontology and duty: the moral obligation of non-abandonment at the neural interface *J. Neural Eng.* **6** 050201

Kim C-S, Ufer S, Seagle C M, Engle C L, Troy Nagle H, Johnson T A and Cascio W E 2004 Use of micromachined probes for the recording of cardiac electrograms in isolated heart tissues *Biosens. Bioelectron.* **19** 1109–16

Kovacs G T A 1994 *Enabling Technologies for Cultured Neural Networks* (San Diego, CA: Academic)

Lai H-Y *et al* 2011 Automatic spike sorting for extracellular electrophysiological recording using unsupervised single linkage clustering based on grey relational analysis *J. Neural Eng.* **8** 036003

Lee I S, Whang C N, Choi K, Choo M S and Lee Y H 2002 Characterization of iridium film as a stimulating neural electrode *Biomaterials* **23** 2375–80

Lempka S F, Miocinovic S, Johnson M D, Vitek J L and McIntyre C C 2009 *In vivo* impedance spectroscopy of deep brain stimulation electrodes *J. Neural Eng.* **6** 046001

Ludwig K A, Uram J D, Yang J, Martin D C and Kipke D R 2006 Chronic neural recordings using silicon microelectrode arrays electrochemically deposited with a poly(3,4-ethylenedioxythiophene) (PEDOT) film *J. Neural Eng.* **3** 59–70

Madou M 1997 *Surface Micromachining* (Boca Raton, FL: CRC Press)

Madou M J 2002 *Fundamentals of Microfabrication: The Science of Miniaturization* (Boca Raton, FL: CRC Press)

Madou M J 2012 *Fundamentals of Microfabrication and Nanotechnology: Manufacturing Techniques and Applications* (Boca Raton, FL: CRC Press)

Maged M E *et al* 2006 Bio-heat transfer model of deep brain stimulation-induced temperature changes *J. Neural Eng.* **3** 306

Maks C B, Butson C R, Walter B L, Vitek J L and McIntyre C C 2009 Deep brain stimulation activation volumes and their association with neurophysiological mapping and therapeutic outcomes *J. Neurol. Neurosurg. Psychiatry* **80** 659–66

Maynard E M, Fernandez E and Normann R A 2000 A technique to prevent dural adhesions to chronically implanted microelectrode arrays *J. Neurosci. Methods* **97** 93–101

McIntyre C C and Grill W 2000 Selective microstimulation of central nervous system neurons *Ann. Biomed. Eng.* **28** 219–33

McIntyre C C and Grill W M 2001 Finite element analysis of the current-density and electric field generated by metal microelectrodes *Ann. Biomed. Eng.* **29** 227–35

McIntyre C C and Grill W M 2002 Extracellular stimulation of central neurons: influence of stimulus waveform and frequency on neuronal output *J. Neurophysiol.* **88** 1592–604

McIntyre C C, Mori S, Sherman D L, Thakor N V and Vitek J L 2004 Electric field and stimulating influence generated by deep brain stimulation of the subthalamic nucleus *Clin. Neurophysiol.* **115** 589–95

McIntyre C C, Grill W M, Sherman D L and Thakor N V 2004a Cellular effects of deep brain stimulation: model-based analysis of activation and inhibition *J. Neurophysiol.* **91** 1457–69

McIntyre C C, Savasta M, Kerkerian-Le Goff L and Vitek J L 2004b Uncovering the mechanism(s) of action of deep brain stimulation: activation, inhibition, or both *Clin. Neurophysiol.* **115** 1239–48

Moffitt M A, McIntyre C C and Grill W M 2004 Prediction of myelinated nerve fiber stimulation thresholds: limitations of linear models *IEEE Trans. Biomed. Eng.* **51** 229–36

Montgomery E B Jr and Gale J T 2008 Mechanisms of action of deep brain stimulation (DBS) *Neurosci. Biobehav. Rev.* **32** 388–407

Moss J, Ryder T, Aziz T Z, Graeber M B and Bain P G 2004 Electron microscopy of tissue adherent to explanted electrodes in dystonia and Parkinson's disease *Brain* **127** 2755–63

Motta P S and Judy J W 2005 Multielectrode microprobes for deep-brain stimulation fabricated with a customizable 3-D electroplating process *IEEE Trans. Biomed. Eng.* **52** 923–33

Newman J 1966 Current distribution on a rotating disk below the limiting current *J. Electrochem. Soc.* **113** 1235–41

Otto K J, Johnson M D and Kipke D R 2006 Voltage pulses change neural interface properties and improve unit recordings with chronically implanted microelectrodes *IEEE Trans. Biomed. Eng.* **53** 333–40

Paik S J, Park Y and Cho D-I 2003 Roughened polysilicon for low impedance microelectrodes in neural probes *J. Micromech. Microeng.* **13** 373–9

Paxinos G and Watson C 2007 *The Rat Brain in Stereotaxic Coordinates* (London: Academic)

Polikov V S, Tresco P A and Reichert W M 2005 Response of brain tissue to chronically implanted neural electrodes *J. Neurosci. Methods* **148** 1–18

Pratap R and Arunkumar A 2007 Material selection for MEMS devices *Indian J. Pure Appl. Phys.* **45** 358–67 (http://eprints.iisc.ernet.in/11720/)

Rattay F 1986 Analysis of models for external stimulation of axons *IEEE Trans. Biomed. Eng.* **33** 974–7

Rattay F 1989 Analysis of models for extracellular fiber stimulation *IEEE Trans. Biomed. Eng.* **36** 676–82

Rousche P J, Pellinen D S, Pivin D P Jr, Williams J C, Vetter R J and Kirke D R 2001 Flexible polyimide-based intracortical electrode arrays with bioactive capability *IEEE Trans. Biomed. Eng.* **48** 361–71

Snow S, Jacobsen S C, Wells D L and Horch K W 2006 Microfabricated cylindrical multielectrodes for neural stimulation *IEEE Trans. Biomed. Eng.* **53** 320–6

Stamatios N S and Peter N S 2007 Assessing the direct effects of deep brain stimulation using embedded axon models *J. Neural Eng.* **4** 107

Subbaroyan J, Martin D C and Kipke D R 2005 A finite-element model of the mechanical effects of implantable microelectrodes in the cerebral cortex *J. Neural Eng.* **2** 103–13

Suner S, Fellows M R, Vargas-Irwin C, Nakata G K and Donoghue J P 2005 Reliability of signals from a chronically implanted, silicon-based electrode array in non-human primate primary motor cortex *IEEE Trans. Neural Syst. Rehab. Eng.* **13** 524–41 PMID: 16425835

Szarowski D H, Andersen M D, Retterer S, Spence A J, Isaacson M, Craighead H G, Turner J N and Shain W 2003 Brain responses to micro-machined silicon devices *Brain Res.* **983** 23–35

Tanghe S J and Wise K D 1992 A 16-channel CMOS neural stimulating array *IEEE J. Solid-State Circuits* **27** 1819–25

Townsend G, Peloquin P, Kloosterman F, Hetke J F and Leung L S 2002 Recording and marking with silicon multichannel electrodes *Brain Res. Protoc.* **9** 122–9

Warman E N, Grill W M and Durand D 1992 Modeling the effects of electric fields on nerve fibers: determination of excitation thresholds *IEEE Trans. Biomed. Eng.* **39** 1244–54

Wei X F and Grill W M 2005 Current density distributions, field distributions and impedance analysis of segmented deep brain stimulation electrodes *J. Neural Eng.* **2** 139

Wei X F and Grill W M 2009 Impedance characteristics of deep brain stimulation electrodes *in vitro* and *in vivo J. Neural Eng.* **6** 046008

Williams J C, Hippensteel J A, Dilgen J, Shain W and Kipke D R 2007 Complex impedance spectroscopy for monitoring tissue responses to inserted neural implants *J. Neural Eng.* **4** 410

Woock J, Yoo P and Grill W 2010 Finite element modeling and *in vivo* analysis of electrode configurations for selective stimulation of pudendal afferent fibers *Brain Res.* **10** 11

Xu J, Shepherd R K, Millard R E and Clark G M 1997 Chronic electrical stimulation of the auditory nerve at high stimulus rates: a physiological and histopathological study *Hear. Res.* **105** 1–29

Yaeli S, Binyamin E and Shoham S 2009 Form-function relations in cone-tipped stimulating microelectrodes *Front. Neuroeng.* **2** 1–8